



Stainless steel wire mesh-supported potassium-doped cobalt oxide catalysts for the catalytic decomposition of nitrous oxide

Laura del Río, Gregorio Marbán *

Instituto Nacional del Carbón (INCAR-CSIC) – c/Francisco Pintado Fe 26, 33011-Oviedo, Spain

ARTICLE INFO

Article history:

Received 23 April 2012

Received in revised form 18 June 2012

Accepted 20 June 2012

Available online 27 June 2012

Keywords:

Co₃O₄

N₂O decomposition

Stainless steel mesh

Potassium

ABSTRACT

Structured catalysts consisting of potassium-doped cobalt oxide supported on stainless steel wire mesh were tested for the decomposition of N₂O under dry and wet conditions. The cobalt oxide catalysts were prepared by the ammonia-evaporation-induced method. Of the several doping procedures tested, dropwise impregnation with potassium carbonate solutions provided the best catalytic results at lower K/Co molar ratios. Kinetic analysis of a potassium-doped catalyst yielded a reaction order on the N₂O partial pressure slightly below unity (0.87). The activation energy values and the natural logarithms of the pre-exponential factors for the different catalysts followed the classical compensation effect. This effect may be the result of a combination of competing reactions on different groups of active centers. Thus, cobalt ions affected by potassium display a low activation energy (~40 kJ/mol), whereas cobalt atoms unaffected by potassium display a higher activation energy equal to that of the undoped catalysts (~106 kJ/mol). The catalytic activity of the catalysts in N₂O decomposition increases with the amount of reducible Co³⁺ ions, although there does not appear to be a direct relation between the amount of Co³⁺ ions and the textural and crystal properties of the catalysts. The addition of water produces some inhibition of the N₂O decomposition reaction on K-doped catalysts, although catalytic activity is completely restored when the water is removed from the reaction stream. The catalysts prepared in this work were found to be among the most active, selective and stable catalysts reported in the literature.

© 2012 Elsevier B.V. All rights reserved.

1. Introduction

Nitrous oxide has been long considered to be as an ozone depletion agent and a greenhouse gas [1]. Well-known anthropogenic sources of N₂O emissions include the adipic acid and nitric acid industries, the fluidised bed combustion of coal and biomass, fertilizer plants and deNO_x treatment techniques, such as SCR and three-way catalysis [2–6]. Awareness of the environmental impact of N₂O has led to an enormous international effort since the Kyoto agreement to reduce anthropogenic N₂O emissions, via a series of clean development mechanism projects [7]. Among the various N₂O reduction techniques considered, thermal decomposition [6,8] and catalytic decomposition [6,9] have been the most widely studied:



It is well known that cobalt-based catalysts present excellent catalytic activities for N₂O decomposition [2,3,10–30]. Typical precursors for cobalt-based catalysts are ion-exchanged

zeolites [3,15,21,22,29] and hydrotalcites [12,28]. The most common cobalt-based catalyst (Co₃O₄ spinel) is fairly stable and suffers no inhibitory effect from the accumulation of oxygen on its surface during reaction at around 300 °C [30]. Doping the cobalt spinel with small amounts of cerium oxide [13] or alkali metals [2,11,14,16] significantly increases the activity of the catalyst. The role of these agents, especially potassium, is to increase the amount of oxygen adsorbed on cobalt ions and to promote the reduction of Co³⁺ to Co²⁺ through an electron donation effect [2,11,16,25,30], thus favouring the desorption of oxygen from the surface of the catalysts, which is the controlling step of N₂O decomposition [13]. Most of these catalysts come in particulate form, and have to be used in packed beds which may lead to uneven gas and temperature distributions and high pressure drops. The use of structured catalysts to overcome these disadvantages, has not been investigated in depth. A study carried out by Pérez-Ramírez et al. [6] on N₂O abatement alternatives in nitric acid plants showed that the structured reactor concept is optimal not only for catalytic N₂O decomposition or reduction in the tail-gas (upstream or downstream of the expander), but also for N₂O decomposition in the process-gas, i.e. below the platinum gauzes. Wang et al. [26] used a ceramic honeycomb support to produce Ni-Co catalysts for N₂O decomposition with good catalytic activity and stability, although

* Corresponding author. Tel.: +34 985119090; fax: +34 985297662.

E-mail address: greca@incar.csic.es (G. Marbán).

in their case the support was crushed before being impregnated with the active phase. In this work we have employed a structured reactor based on a novel concept, initially tested for the preferential oxidation of carbon monoxide [31] and the catalytic decomposition of methanol [32]. The reactor consists of a very fine stainless steel wire mesh, coated with mesoporous Co_3O_4 nanowires (catalyst), and rolled up inside a stainless steel pipe (1/4" o.d.). In this kind of reactor, the metal wire mesh provides a large geometric surface area for supporting the catalyst. It also guarantees a negligible pressure drop and good heat transfer through the reactor. In the present study the mesh-supported catalyst was modified with potassium in order to produce the desired increase in catalytic activity. The catalysts obtained were tested for N_2O decomposition in the presence of oxygen and water.

2. Experimental

2.1. Catalyst synthesis

Wire mesh-supported cobalt oxide catalysts were prepared by the ammonia-evaporation-induced method at 90°C for 18 h using $\text{Co}(\text{NO}_3)_2 \cdot 6\text{H}_2\text{O}$ as cobalt precursor. A detailed description of the synthesis procedure can be found elsewhere [31,32].

Two types of stainless steel wire mesh were tested as catalyst supports: M40 (30 μm wire diameter and 40 μm screen opening; smooth fabric) and M25 (25 μm wire diameter and 25 μm screen opening; twill fabric). Before use, both meshes were washed with HNO_3 (4 M) at 60°C for 4 h and then with isopropyl alcohol in an ultrasonic bath for 10 min.

The uncalcined wire mesh-supported cobalt hydroxide catalysts were impregnated with potassium by the dropwise addition of an aqueous solution of K_2CO_3 (0.15–0.21 M) or KOH (0.231 M). After wetting the sample, the excess solution was removed by applying an air stream, followed by vacuum-drying at 60°C for 1 h. The impregnation step was then repeated in order to obtain the desired amount of potassium. The molar ratio of potassium to cobalt (K/Co) ranged between 0 and 0.03. In some specific cases potassium addition was performed by equilibrium impregnation. In this case each sample was immersed in aqueous KOH solutions (0.21 M) and kept under magnetic stirring for several hours. Afterwards, the metal wire mesh was removed from the solution, thoroughly washed with deionised water and vacuum-dried at 60°C .

2.2. Finally all the samples were calcined in air at 400°C for 2 h

The samples were denoted as M-KP-IM-K/Co where M refers to the type of stainless steel wire mesh (M40 or M25), KP is the potassium precursor (KC for potassium carbonate; KO for potassium hydroxide), IM is the impregnation method (DW for dropwise impregnation; EA for equilibrium adsorption impregnation) and K/Co is the molar ratio of the doped metal (from 0.006 to 0.029). Undoped catalysts were simply denoted M25 or M40.

2.3. Catalyst characterisation

The metal contents of the samples were determined by atomic absorption spectroscopy (AAS) and mass spectrometry (ICP-MS). Microscopic images of the samples were obtained using a scanning electron microscope (Zeiss, DSM 942 model). X-ray diffraction (XRD) analyses were carried out with a Bruker instrument (D8 Advance) operating at 40 kV and 40 mA and using $\text{Cu K}\alpha$ radiation ($\lambda = 0.15406 \text{ nm}$). Crystal size values (d_{XRD}) were estimated from the XRD patterns by means of Scherrer's equation. The instrumental contribution to line broadening was taken into account by using the diffraction pattern of corundum as instrumental standard.

TPR analyses were performed in a chemisorption analyzer (Autochem II) equipped with a TCD detector. For each analysis approximately 80 mg of sample was pre-treated at 400°C for 1 h in an argon flow, cooled down to room temperature and then treated with a 50 mL/min stream of 10 vol% H_2 in argon from 100 to 600°C at $5^\circ\text{C}/\text{min}$.

N_2 adsorption isotherms at -196°C were obtained in a Micromeritics ASAP 2010 volumetric adsorption system. The BET surface area was determined from the isotherm analysis in the relative pressure range of 0.04–0.20.

2.4. Catalytic activity tests

Catalytic activity tests for N_2O decomposition were performed in a six-flow parallel microrreactor system that allows up to six samples to be simultaneously tested by means of an automatically operated multiposition valve. Each catalyst consisted of a 5 cm \times 1 cm strip that was rolled up to form a 1 cm-high cylindrical piece. One roll of catalyst was then inserted into each of the six stainless-steel reactors (1/4 in. outer diameter). A stream composed of 1300 ppm N_2O , 0.5 vol% O_2 , 0 or 4 vol% H_2O and 10 vol% Ar in helium was fed into each reactor at a gas hourly space velocity of $\sim 20,000 \text{ h}^{-1}$. Weight hourly space velocities varied in the range $0.08 - 0.10 \text{ g}_{\text{N}_2\text{O}} \text{ g}_{\text{cat}}^{-1} \text{ h}^{-1}$, depending on the amount of catalyst loaded onto the metal wire mesh. The samples were first heated in a flow of He at 400°C for 30 min. Then the reactant stream was passed through the catalysts and their catalytic activity and selectivity were evaluated at decreasing temperatures from 400 to 300°C , in 3 h isothermal steps. It was generally found that 30 min after each change in conditions the conversion levels were constant and were thus considered as steady-state values. The transition ramp between each temperature step was performed under a helium atmosphere. The products were analysed on-line by mass spectrometry (OmniStar 3000). N_2O , N_2 , O_2 , and H_2O were quantitatively analysed with the help of previous calibration steps, whereas the evolution of NO and NO_2 was followed from the changes in the mass intensities of the fragments 15 (NO) and 46 (NO_2). By means of this procedure it was possible to know for certain whether any products other than N_2 were formed during the reaction. The conversion parameter, X, represents the fraction of N_2O converted to N_2 and O_2 according to the reaction:



Each experimental conversion point was evaluated after two hours of reaction at the specified temperature. For the kinetic analysis, experiments at different N_2O partial pressures (0.17–0.40 atm) and temperatures (150 – 300°C) were performed. The following potential equation for the reaction rate was used to fit the experimental results:

$$-\frac{dP_{\text{N}_2\text{O}}}{dt} = kP_{\text{N}_2\text{O}}^n \quad (1)$$

where $P_{\text{N}_2\text{O}}$ is the outlet partial pressure of N_2O , n is the reaction order and k is the reaction rate constant, that follows an apparent Arrhenius-type dependence; $k = k_0 \exp[-E_a/(RT)]$. Integral reactor behaviour was employed to solve Eq. (1) and the following expression was used to calculate the values for the reaction rate constant:

$$k = \frac{F_{\text{N}_2\text{O}}^0}{w_{\text{cat}} (P_{\text{N}_2\text{O}}^0)^n} \frac{1 - (1 - X)^{1-n}}{1 - n} \quad (2)$$

Only conversion values below 0.7 were used in this equation.

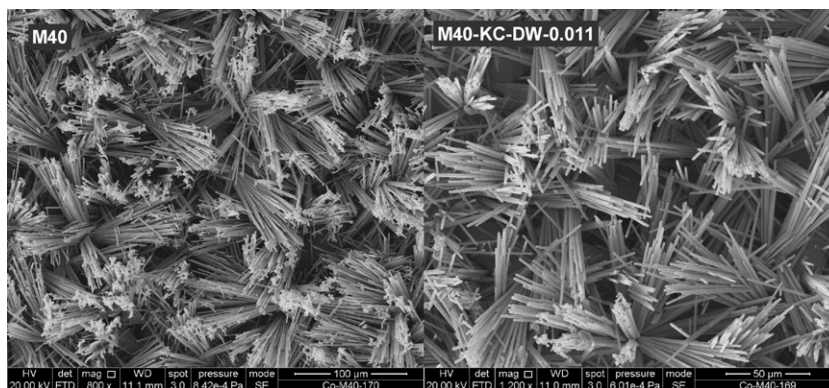


Fig. 1. SEM images of samples M40 and M40-KC-DW-0.011.

3. Results and discussion

3.1. Structural characterisation

Fig. 1 shows SEM images of samples M40 and M40-KC-DW-0.011. The samples show typical flower-like mesoporous nanowire arrays evenly spaced over the metal wire meshes [31]. K-doping does not produce any noticeable macroscopic change in the spinel arrays, as can be observed in figure. The Co_3O_4 yield for all the mesh-supported catalysts prepared in this work was 46 ± 4 wt%. Fig. 2 shows the XRD spectrum for an undoped sample (M40) and the samples doped with potassium after dropwise impregnation with potassium carbonate solutions. All the visible peaks are ascribed to the Co_3O_4 spinel. K_2O was not detected as a separate phase in the XRD plots. As can be seen in Fig. 2, the addition of potassium causes a widening of the Co_3O_4 peaks which is due to the smaller size of the crystals in the spinel. This was evaluated by

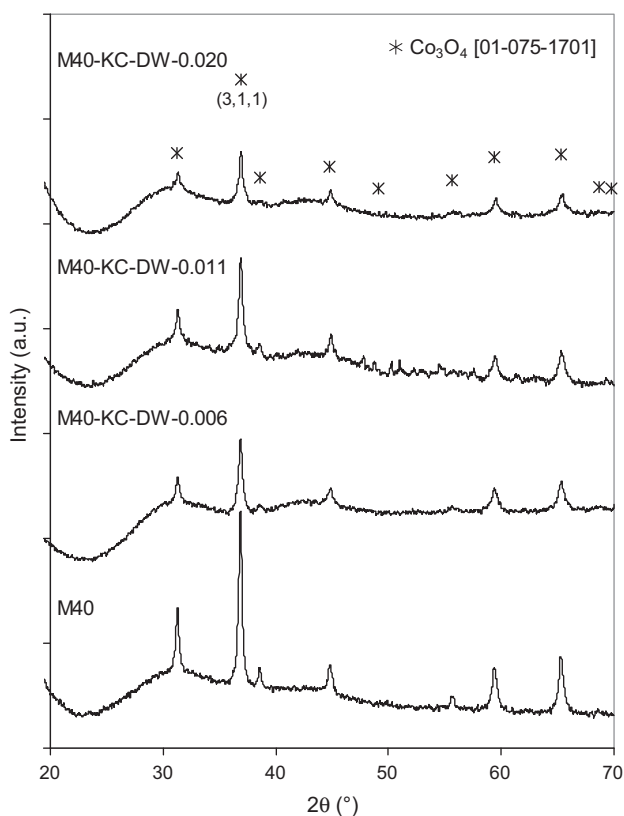


Fig. 2. XRD spectra of M40 mesh-supported catalysts.

means of the Scherrer equation and the results were plotted against the K/Co molar ratio in Fig. 3. It can be seen that the crystal size diminishes from ~ 27 to ~ 21 nm when a small amount of potassium ($\text{K/Co} = 0.006$) is added, but remains unchanged for higher loads of potassium, up to $\text{K/Co} = 0.020$. In contrast, the specific surface area evaluated by N_2 physisorption, follows a different trend: there is a slight diminution for the lowest potassium load ($\text{K/Co} = 0.006$) followed by a steady growth for higher potassium loads (Fig. 3) up to a value of $52 \text{ m}^2/\text{g}$. This trend is similar to that found by other authors using potassium-doped Co_3O_4 catalysts prepared by the calcination of KNO_3 -impregnated cobalt carbonate [10]. There is apparently no correspondence between the variation in crystal size and BET surface area as the K/Co molar ratio increases. A minimum amount of potassium causes the $\text{Co}(\text{OH})_2$ to transform during calcination into slightly smaller Co_3O_4 crystals, but, as the potassium load increases, its main role is to prevent these crystals from forming large aggregates. Thus, assuming a perfectly spherical geometry and a Co_3O_4 density of 6.1 g/cm^3 , the number of crystals per particle decreases from ~ 5 to ~ 1 when the K/Co molar ratio increases from 0.006 to 0.020.

3.2. Reaction kinetics of the potassium doped catalysts

In order to compare the activities of the catalysts both with each other and with catalysts described in the literature, a kinetic analysis was performed on the catalyst M40-KC-DW-0.011, by applying the potential equation presented in the experimental section. The reaction rate was assumed to be of zero order with respect to the oxygen partial pressure, as is usually the case for cobalt-based catalysts [3]. The best fittings for the different N_2O partial pressures (0.17–0.50 atm) were obtained for $n = 0.87$;

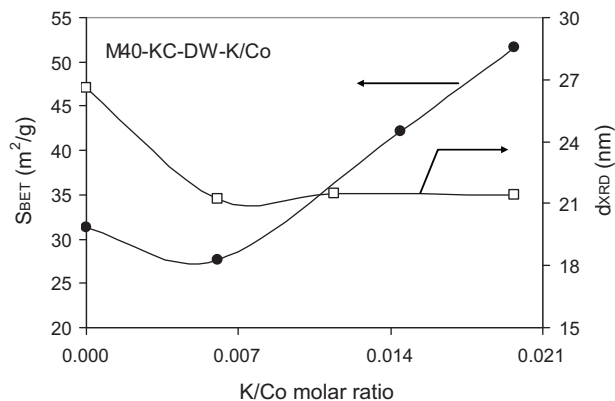


Fig. 3. Variation of BET surface area and crystal size (d_{XRD} evaluated by Scherrer's equation) with the potassium content for the M40 mesh-supported catalysts.

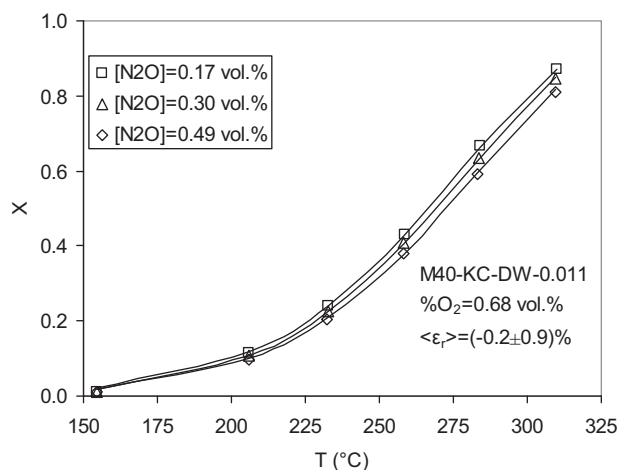


Fig. 4. Kinetic experiments performed for M40-KC-DW-0.011. Solid lines represent the fitting to the potential Eq. (1) for $n = 0.87$.

$k_0 = 83.8 \text{ mol g}_{\text{cat}}^{-1} \text{ s}^{-1} \text{ atm}^{-0.87}$ and $E_a = 60.1 \text{ kJ/mol}$. Fig. 4 shows a comparison between the experimental results and the model predictions. As can be seen a very low average relative error of $-0.2 \pm 0.9\%$ was obtained. The reaction order was found to be slightly lower than 1 (0.87). This may be due to the almost negligible but still noticeable effect that the adsorption of N_2O by the active centers has upon the reaction rate in N_2O decomposition (Langmuir–Hinshelwood kinetics). This effect was not observed by Kapteijn et al. [3] although their analyses were performed at higher temperatures ($400\text{--}500^\circ\text{C}$) than those used in this work ($150\text{--}350^\circ\text{C}$). No formation of NO or NO_2 was observed in any of the experiments in this study at temperatures below 400°C . The value of selectivity to N_2 was, therefore, unity.

3.3. Type of support and impregnation method

Fig. 5 shows the plots of N_2O conversion versus reaction temperature for catalysts prepared with the different supports (M25 and M40 meshes) and the impregnation procedures (equilibrium impregnation with KOH solutions and dropwise addition of KOH and K_2CO_3 solutions). The undoped catalysts presented very similar catalytic activities regardless of the kind of mesh used as support. On the other hand, the potassium-doped catalysts performed

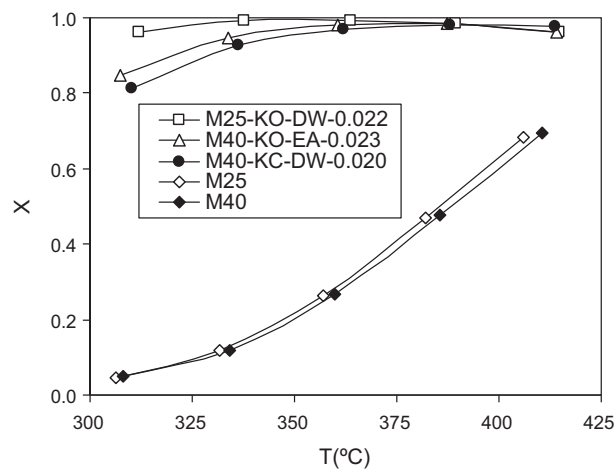


Fig. 5. N_2O conversion plots for catalysts prepared with different supports and impregnation procedures ($F_{\text{N}_2\text{O}}/w_{\text{cat}} \sim 5 \times 10^{-7} \text{ mol mg}^{-1} \text{ s}^{-1}$; $p_{\text{N}_2\text{O}}^0 = 0.13 \text{ atm}$; $p_{\text{O}_2}^0 = 0.5 \text{ atm}$).

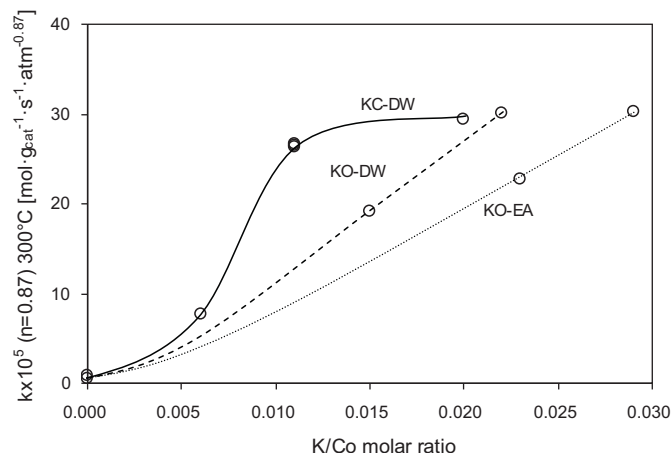


Fig. 6. Variation of the reaction rate constant k with the K/Co molar ratio for catalysts prepared with different supports and impregnation procedures ($F_{\text{N}_2\text{O}}/w_{\text{cat}} \sim 5 \times 10^{-7} \text{ mol mg}^{-1} \text{ s}^{-1}$; $p_{\text{N}_2\text{O}}^0 = 0.13 \text{ atm}$; $p_{\text{O}_2}^0 = 0.5 \text{ atm}$).

much better, achieving conversions of over 0.98 at temperatures of around 350°C . In principle, the catalyst prepared by the dropwise addition of a KOH solution seems to be the most active of all the potassium-doped catalysts. However, small differences in the active phase weight, N_2O molar flow and K/Co molar ratio (which are unavoidable given the kind of reaction setup and preparation methods used in this work) make it difficult to use conversion values similar to those displayed in Fig. 5 in order to be able to rank the catalysts according to their catalytic activity. To circumvent this drawback, the reaction rate constants were evaluated by means of Eq. (2), the reaction order being evaluated by the kinetic analysis ($n = 0.87$). Fig. 6 shows the variation in the reaction rate at 300°C under dry conditions with the increase in the K/Co molar ratio, for the catalysts prepared with different impregnation procedures. For the most active catalysts, for which the conversion values at 300°C were close to unity, the reaction rate constants at 300°C were evaluated by means of the Arrhenius equation. As can be seen, the dropwise impregnation of potassium carbonate yielded higher values of catalytic activity at lower K/Co molar ratios than KOH impregnation. Fig. 7 shows that the addition of potassium causes

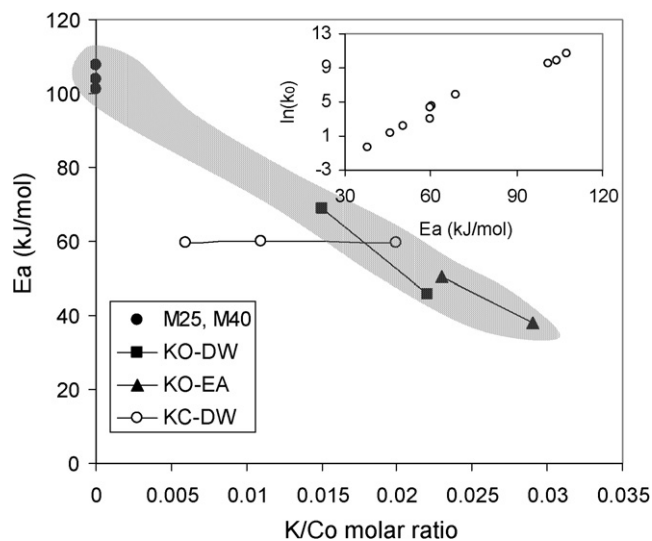


Fig. 7. Values of activation energy obtained by applying the Arrhenius equation to the values of k (Eq. (2); $n = 0.87$) corresponding to the catalysts prepared with different impregnation procedures and tested at dry conditions ($F_{\text{N}_2\text{O}}/w_{\text{cat}} \sim 5 \times 10^{-7} \text{ mol mg}^{-1} \text{ s}^{-1}$). Inset: compensation effect plot.

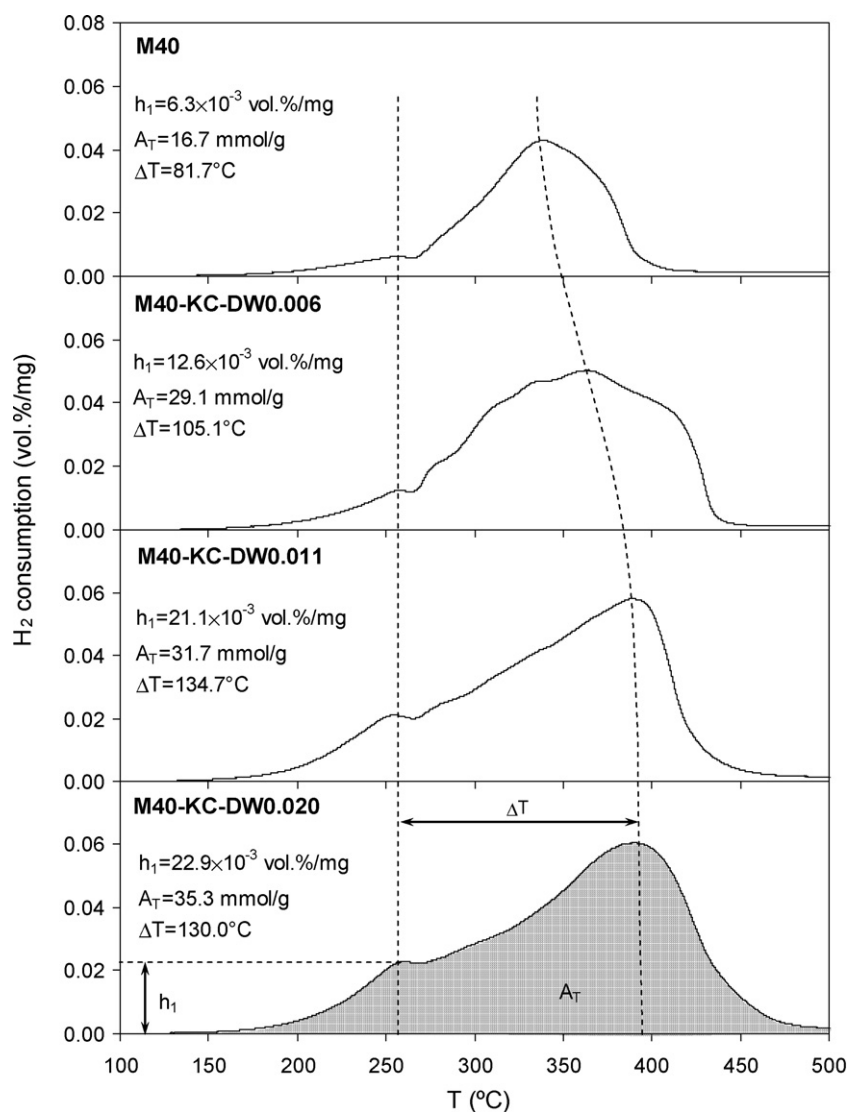


Fig. 8. TPR plots (10 vol% H_2/Ar) for catalysts prepared with different K/Co molar ratios.

a decrease in the apparent activation energy of the N_2O decomposition reaction. In the absence of potassium, the activation energy values (104–108 kJ/mol) are identical to those found by Kapteijn et al. [3] using cobalt-exchanged zeolites (106 kJ/mol). Upon the addition of potassium, the activation energy obtained under dry conditions drops to values as low as 38 kJ/mol (K/Co = 0.029). The activation energy obtained with the catalysts impregnated with KOH experiences a linear decrease as the potassium content of the catalysts increases (Fig. 7), whereas the catalysts impregnated with potassium carbonate undergo a marked decrease at a low K/Co value (0.006) although the activation energy remains thereafter constant for increasing potassium contents (Fig. 7). In the light of this result it is clear that potassium not only causes variations in the textural properties and crystal size of the cobalt-based catalysts (Fig. 3), which may alter the number of initial active centers for catalysis, but also changes the enthalpy of activation of the cobalt centers. The inset in Fig. 7 shows the variation in the apparent activation energy together with the natural logarithm of the pre-exponential factor k_0 . The quasi-linear relation displayed by the data is often encountered in heterogeneous reactions and has been known, since the beginning of the 20th century, as the compensation effect [33,34] of kinetic parameters or the theta rule [35]. In the literature many attempts have been made to explain this

effect, most of which have met with only limited success. However a particularly interesting explanation was proposed by Nicholas [36] and Bagg [34], who suggested that the compensation effect occurs when the global reaction is a combination of competing reactions that take place on different groups of active centers with each group displaying a different value of activation energy and a different pre-exponential factor. According to this theory it is the varying proportions of these groups of active centers that causes the variation in the apparent activation energies and pre-exponential factors for the global reaction rate. In the case of the potassium-doped catalysts it can be assumed that the potassium atoms change the electronic configuration of the active centers, as described by the group of Inoue [2,10]. Thus, the cobalt ions affected by potassium would display a lower activation energy, whereas the cobalt atoms unaffected by potassium would exhibit an activation energy equal to that of the undoped catalysts.

To obtain a further insight into the reaction mechanism, TPR analyses were performed with the catalysts prepared by dropwise impregnation with potassium carbonate. Fig. 8 shows the TPR plots obtained. As can be seen, there are two reduction peaks at around 250 °C and 350–400 °C. The first peak is attributed to the reduction of Co^{3+} to Co^{2+} [10] and is independent of the addition of K. The high temperature peak which is ascribed to the reduction of

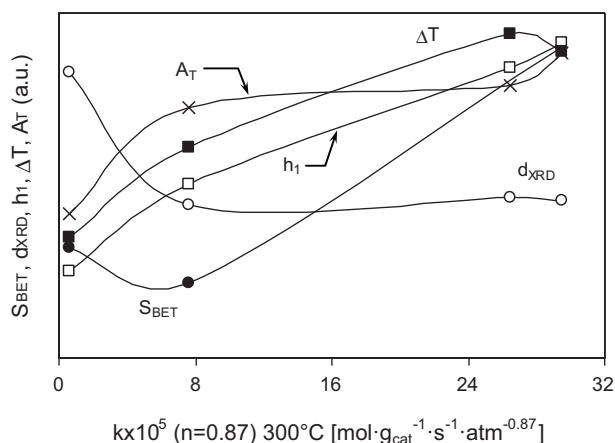


Fig. 9. Variation of S_{BET} , d_{XRD} , h_1 , ΔT and A_T with the reaction rate constant, k (Eq. (2); $n=0.87$), corresponding to the catalysts prepared with different K/Co molar ratios ($F_{\text{N}_2\text{O}}/W_{\text{cat}} \sim 5 \times 10^{-7} \text{ mol mg}^{-1} \text{ s}^{-1}$).

Co^{2+} to metallic Co [10] shifts towards high temperatures upon the addition of K. Fig. 8 also shows the values of three parameters for the different TPR plots: h_1 , representing the height of the first peak, A_T , the total area under the TPR curve (specific hydrogen consumption) and ΔT , the difference in temperature between the first and second peaks. The values for all these parameters, together with those of specific surface area (S_{BET}) and crystal size (d_{XRD}) are plotted in Fig. 9 against the reaction rate constant at 300 °C. As can be seen the best correlations are obtained for the variations of h_1 and ΔT with k . It is thought that Co^{2+} is oxidised to Co^{3+} by the oxygen atom formed during the decomposition of N_2O . The resulting Co^{3+} must be reduced to Co^{2+} to regenerate the active sites. The results shown in Figs. 8 and 9 suggest that the interaction between K and Co_3O_4 increases the number of active sites available to undergo the $\text{Co}^{3+}/\text{Co}^{2+}$ redox cycle for the reduction of N_2O (h_1 , A_T) and

averts the unwanted Co^{2+} reduction by shifting it towards high temperatures (ΔT).

3.4. Effect of water in the reaction stream

Fig. 10 shows the variation of N_2O conversion (X) with temperature for the catalysts doped by impregnation with potassium carbonate solutions. The experiments comprised three consecutive steps: step 1, when there is no H_2O in the gas stream, step 2, when 4 vol% H_2O is added to the reaction stream and step 3, after the water has been removed from the reaction stream. As can be seen, the undoped catalyst undergoes strong deactivation after being exposed to water, whereas the doped catalysts only experience some inhibition in the presence of water, especially at low temperatures. However catalytic activity is fully restored in step 3 for the catalysts with K/Co molar ratios over 0.006. Water vapour competes with N_2O for adsorption onto the same active centers. However it may also cause some loss of active surface area in the undoped catalyst which is reduced by the presence of potassium. The total recovery of activity displayed by the potassium-doped catalyst is another indication of the high stability of these catalysts.

3.5. Comparison with other cobalt-based catalysts described in the literature

Data from a survey of cobalt-based catalysts for N_2O decomposition are provided in Table 1 (undoped catalysts) and 2 (potassium-doped catalysts). The values of the kinetic rate constant at 300 °C for these catalysts were obtained by applying Eq. (2), for $n=0.87$, to the conversion values extracted with a Visual-basic program [37] from digital images of the conversion plots included in the referenced works. It should be pointed out that all the catalysts included in tables were in particulate form and tested in fixed-bed reactors. The catalysts prepared in the present study are in monolithic form and permit a high heat exchange rate (metallic support) and a low pressure drop during the reaction. As can be seen in Table 1, only one undoped catalyst [14] presents a higher catalytic

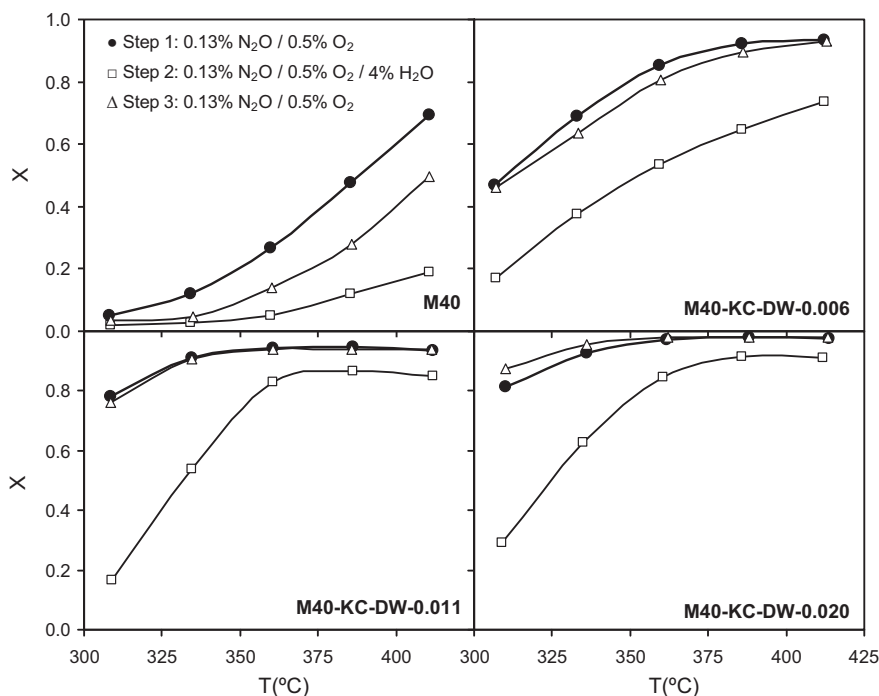


Fig. 10. N_2O conversion plots for sequential experiments (1–without water; 2–with water; 3–without water) performed with catalysts prepared with different K/Co molar ratios ($F_{\text{N}_2\text{O}}/W_{\text{cat}} \sim 5 \times 10^{-7} \text{ mol mg}^{-1} \text{ s}^{-1}$).

Table 1Studies with undoped cobalt-based catalysts for N₂O decomposition.

Ref.	Catalyst precursor	Catalyst shape	Gas stream composition	$k \times 10^5$ ($n = 0.87$) 300 °C $\text{mol}_{\text{gcat}}^{-1} \text{s}^{-1} \text{atm}^{-0.87}$
[14]	Co(NO ₃) ₂ precipitated with Na ₂ CO ₃ and calcined at 400 °C	Particles	0.25 vol% N ₂ O 0.00 vol% O ₂	3.6
M25 This work	Hydrothermally treated Co(NO ₃) ₂ calcined at 400 °C	M25 mesh-supported catalyst	0.13 vol% N ₂ O 0.50 vol% O ₂	0.8
M40 This work		M40 mesh-supported catalyst		0.6
[2]	CoCO ₃ calcined at 400 °C	Particles 0.8–2.0 mm	0.5 vol% N ₂ O 2.0 vol% O ₂	0.6
[10]	CoCO ₃ calcined at 400 °C			0.5
[12]	Hydrotalcite calcined at 700 °C	Particles 0.25–0.42 mm	0.05 vol% N ₂ O 0.00 vol% O ₂	0.1

Table 2Studies with potassium-doped cobalt-based catalysts for N₂O decomposition.

Ref.	Catalyst precursor	Doping agent	K/Co molar ratio	Catalyst shape	Gas stream composition	$k \times 10^5$ ($n = 0.87$) 300 °C $\text{mol}_{\text{gcat}}^{-1} \text{s}^{-1} \text{atm}^{-0.87}$
[10]	CoCO ₃ calcined at 400 °C	KNO ₃	0.050	Particles 0.8–2.0 mm	0.5 vol% N ₂ O 2.0 vol% O ₂	69.8
[2]	CoCO ₃ calcined at 400 °C	KOH KNO ₃ KHCO ₃ CH ₃ COOK K ₂ SO ₄ KCl	0.020			43.8 40.7 36.7 35.1 6.5 3.5
[12]	Hydrotalcite calcined at 700 °C	KNO ₃	0.040	Particles 0.25–0.42 mm	0.05 vol% N ₂ O 0.00 vol% O ₂	18.4
M25-KO-DW-0.022 This work	Hydrothermally treated Co(NO ₃) ₂ calcined at 400 °C	KOH (Dropwise impregnation)	0.022	M25 mesh-supported catalyst	0.13 vol% N ₂ O 0.50 vol% O ₂	30.2
M40-KO-EA-0.023 This work		KOH (Equilibrium impregnation)	0.023	M40 mesh-supported catalyst		22.8
M40-KC-DW-0.006 This work		K ₂ CO ₃ (Dropwise impregnation)	0.006			7.6
M40-KC-DW-0.011 This work			0.011		0.17–0.50 vol% N ₂ O 0.50–0.70 vol% O ₂	26.5
M40-KC-DW-0.020 This work			0.020		0.16 vol% N ₂ O 0.70 vol% O ₂	29.5

activity than the undoped catalysts prepared in our study (M25 and M40). The former catalyst, tested in the absence of oxygen [14], was prepared via precipitation with Na₂CO₃. It may therefore contain a residual amount of sodium, which could be the cause of the high catalytic activity.

Table 2 shows the values for the reaction rate constant for N₂O decomposition at 300 °C corresponding to the potassium-doped catalysts prepared in this work together with those of other potassium-doped catalysts described in the literature [2,10,12]. The best structured catalysts in our study show values of catalytic activity that match those of the best particulate catalysts reported in the literature. The monolithic configuration of these catalysts, together with their high activity, selectivity, stability and water-resistance make them highly suitable for decomposing N₂O.

4. Conclusions

In summary, the structured catalysts prepared in this work were found to be among the most active, selective and stable catalysts reported in the literature. In the preparation of the catalysts it was found that dropwise impregnation with potassium carbonate solutions provided the best catalytic results at lower K/Co molar ratios. Kinetic analysis of the reactions under dry conditions for the different catalysts showed a correlation between the values of activation energy and the natural logarithms of the pre-exponential factors. This effect may be the result of the combination of competing reactions that take place on the different groups of active centers. Thus, the cobalt ions affected by potassium displayed a low activation energy (~40 kJ/mol), whereas the cobalt atoms unaffected by potassium exhibited a higher activation energy equal to that of

the undoped catalysts (~106 kJ/mol). It was also observed that catalytic activity in N₂O decomposition increases with the amount of reducible Co³⁺ ions. The addition of water produces some inhibition of the N₂O decomposition reaction on the K-doped catalysts, although catalytic activity is completely restored when the water is removed from the reaction stream.

Acknowledgements

The financial support for this research work provided by the Spanish MEC (CTQ2011-24776) is gratefully acknowledged. Funding through the FICYT Regional Project IB08-103 is also acknowledged.

References

- [1] H. Rodhe, *Science* 248 (1990) 1217–1219.
- [2] H. Yoshino, C. Ohnishi, S. Hosokawa, K. Wada, M. Inoue, *Journal of Materials Science* 46 (2011) 797–805.
- [3] F. Kapteijn, G. Marbán, J. Rodríguez-Mirasol, J.A. Moulijn, *Journal of Catalysis* 167 (1997) 256–265.
- [4] F. Kapteijn, G. Mul, G. Marbán, J. Rodríguez-Mirasol, J.A. Moulijn, in: 11Th International Congress on Catalysis – 40Th Anniversary, *Studies in Surface Science and Catalysis* 101 (1996) 641–650.
- [5] H. Zhou, J. Lu, H. Zhou, *Journal of Engineering for Thermal Energy and Power* 15 (2000) 1–3.
- [6] J. Pérez-Ramírez, F. Kapteijn, K. Schöffel, J.A. Moulijn, *Applied Catalysis B: Environmental* 44 (2003) 117–151.
- [7] S.J. Lee, I.S. Ryu, B.M. Kim, S.H. Moon, *International Journal of Greenhouse Gas Control* 5 (2011) 167–176.
- [8] G. Marbán, F. Kapteijn, J.A. Moulijn, *Combustion and Flame* 107 (1996) 103–113.
- [9] F. Kapteijn, J. Rodríguez-Mirasol, J.A. Moulijn, *Applied Catalysis B: Environmental* 9 (1996) 25–64.
- [10] K. Asano, C. Ohnishi, S. Iwamoto, Y. Shiota, M. Inoue, *Applied Catalysis B: Environmental* 78 (2008) 242–249.

- [11] G. Maniak, P. Stelmachowski, F. Zasada, W. Piskorz, A. Kotarba, Z. Sojka, *Catalysis Today* 176 (2011) 369–372.
- [12] H. Cheng, Y. Huang, A. Wang, L. Li, X. Wang, T. Zhang, *Applied Catalysis B: Environmental* 89 (2009) 391–397.
- [13] L. Xue, C. Zhang, H. He, Y. Teraoka, *Applied Catalysis B: Environmental* 75 (2007) 167–174.
- [14] N. Pasha, N. Lingaiah, N.S. Babu, P.S.S. Reddy, P.S.S. Prasad, *Catalysis Communications* 10 (2008) 132–136.
- [15] R.S. da Cruz, A.J.S. Mascarenhas, H.M.C. Andrade, *Applied Catalysis B: Environmental* 18 (1998) 223–231.
- [16] P. Stelmachowski, G. Maniak, A. Kotarba, Z. Sojka, *Catalysis Communications* 10 (2009) 1062–1065.
- [17] Q. Shen, L. Li, J. Li, H. Tian, Z. Hao, *Journal of Hazardous Materials* 163 (2009) 1332–1337.
- [18] K. Karásková, L. Obalová, K. Jiráťová, F. Kovanda, *Chemical Engineering Journal* 160 (2010) 480–487.
- [19] L. Xue, C. Zhang, H. He, Y. Teraoka, *Catalysis Today* 126 (2007) 449–455.
- [20] L. Obalová, G. Maniak, K. Karásková, F. Kovanda, A. Kotarba, *Catalysis Communications* 12 (2011) 1055–1058.
- [21] M.C. Campa, V. Indovina, D. Pietrogiaconi, *Applied Catalysis B: Environmental* 91 (2009) 347–354.
- [22] M.F. Fellah, I. Onal, *Catalysis Today* 137 (2008) 410–417.
- [23] N. Russo, D. Fino, G. Saracco, V. Specchia, *Catalysis Today* 119 (2007) 228–232.
- [24] C.H. Ohnishi, K. Asano, H.J. Jeon, S. Hosokawa, S. Iwamoto, M. Inoue, *Polyhedron* 28 (2009) 1295–1300.
- [25] F. Zasada, P. Stelmachowski, G. Maniak, J.F. Paul, A. Kotarba, Z. Sojka, *Catalysis Letters* 127 (2009) 126–131.
- [26] Y. Wang, J. Zhang, J. Zhu, J. Yin, H. Wang, *Energy Conversion and Management* 50 (2009) 1304–1307.
- [27] K. Karásková, L. Obalová, F. Kovanda, *Catalysis Today* 176 (2011) 208–211.
- [28] L. Obalová, K. Karásková, K. Jiráťová, F. Kovanda, *Applied Catalysis B: Environmental* 90 (2009) 132–140.
- [29] X. Zhang, Q. Shen, C. He, Y. Wang, J. Cheng, Z. Hao, *Journal of Hazardous Materials* 192 (2011) 1756–1765.
- [30] C. Ohnishi, K. Asano, S. Iwamoto, K. Chikama, M. Inoue, *Catalysis Today* 120 (2007) 145–150.
- [31] G. Marbán, I. López, T. Valdés-Solís, A.B. Fuertes, *International Journal of Hydrogen Energy* 33 (2008) 6687–6695.
- [32] G. Marbán, A. López, I. López, T. Valdés-Solís, *Applied Catalysis B: Environmental* 99 (2010) 257–264.
- [33] Y. Moro-Oka, A. Ozaki, *Journal of Catalysis* 10 (1968) 84–86.
- [34] J. Bagg, *Journal of Catalysis* 16 (1970) 377–385.
- [35] G.M. Schwab, *Journal of Catalysis* 84 (1983) 1–7.
- [36] J.F. Nicholas, *Journal of Chemical Physics* 31 (1959) 922–925.
- [37] I. López, T. Valdés-Solís, G. Marbán, *International Journal of Hydrogen Energy* 33 (2008) 197–205.